WISE: Low-Cost Wide Band Spectrum Sensing Using UWB

Zhicheng Luo
Southern University of Science and Technology & Peng Cheng Laboratory
Shenzhen, China

Qianyi Huang
Sun Yat-sen University & Peng Cheng Laboratory
Guangzhou, China

Rui Wang
Southern University of Science and Technology
Shenzhen, China

Hao Chen
Peng Cheng Laboratory
Shenzhen, China

Xiaofeng Tao
Beijing University of Posts and Telecommunications & Peng Cheng Laboratory
Beijing, China

Guihai Chen
Shanghai Jiao Tong University
Shanghai, China

Qian Zhang
Hong Kong University of Science and Technology
Hong Kong, China

ABSTRACT

Spectrum sensing plays a crucial role in spectrum monitoring and management. However, due to the expensive cost of high-speed ADCs, wideband spectrum sensing is a long-standing challenge. In this paper, we present how to transform Ultra-wideband (UWB) devices into a spectrum sensor which can provide wideband spectrum monitoring at a low cost. Compared with the expensive high-speed ADCs which cost at least hundreds of dollars, a UWB device is only several dollars. As the low-cost UWB technology is not originally designed for spectrum sensing, we address the inherent limitations of low-cost devices such as limited memory, low SPI speed and low accuracy, and show how to obtain spectrum occupancy information from the noisy and spurious UWB channel impulse response. In this paper, we present *WISE*, which not only can give accurate channel occupancy information, but also can precisely estimate the signal power and bandwidth. *WISE* can also detect fleeting radar signals. We implement *WISE* and perform extensive evaluations with both controlled experiments and field tests. Results show that *WISE* can sense up to 900MHz bandwidth and the power estimation error is less than 3dB. *WISE* can also accurately detect busy 5G channels. We believe that *WISE* provides a new paradigm for low-cost wideband spectrum sensing, which is critical for large-scale fine-grained spectrum monitoring.

CCS CONCEPTS

• **Networks** → **Network monitoring**; **Mobile networks**.

SenSys '22, November 6–9, 2022, Boston, MA, USA

ACM ISBN 978-1-4503-9886-2/22/11…$15.00
https://doi.org/10.1145/3560905.3568541

KEYWORDS

Spectrum sensing, UWB, Low-cost, Wideband

ACM Reference Format:
Zhicheng Luo, Qianyi Huang, Rui Wang, Hao Chen, Xiaofeng Tao, Guihai Chen, and Qian Zhang. 2022. *WISE*: Low-Cost Wide Band Spectrum Sensing Using UWB. In *The 20th ACM Conference on Embedded Networked Sensor Systems (SenSys '22), November 6–9, 2022, Boston, MA, USA.* ACM, New York, NY, USA, 16 pages. https://doi.org/10.1145/3560905.3568541

1 INTRODUCTION

With the unprecedented amount of wireless traffic and rapidly increasing number of untethered devices, the limited spectrum has been recognized as a scarce, valuable resource. The key to addressing the spectrum scarcity issue is to have a better understanding of the spectrum usage pattern, that is, global information about which channel is occupied/available in both spatial and temporal domains. Thus, city-level fine-grained spectrum monitoring is of vital importance to help regulators make strategic allocations. It is also the key to the success of dynamic spectrum access, where the spectrum is shared among multiple radio access technologies (RATs). For example, in the US, Wi-Fi 6E and 5G New Radio Unlicensed (NR-U) will share the unlicensed 6GHz band [19], where the whole bandwidth is 1200MHz (5925 − 7125MHz); LTE/5G and military radar are sharing the 150MHz CBRS band at 3.5GHz [18].

However, wideband spectrum sensing has been a long-standing challenge. As we know, wideband spectrum sensing requires high-speed ADCs, which are too expensive to be widely affordable. Prior works have proposed several solutions [24, 35, 39, 46], where a low-speed ADC scans a portion of the spectrum each time and stitches the results to generate a wideband spectrum map. Such design principles naturally lead to the drawback that transient signals (e.g., radar) can be easily missed. Researchers also combine software-defined radios with signal processing techniques (e.g., sparse Fourier transform [20, 25, 26]) and advanced scanning strategies [24, 39, 46] to provide wideband spectrum sensing. Unfortunately, they are feasible only when the spectrum is sparsely occupied, which is not always true given the ever-increasing demand

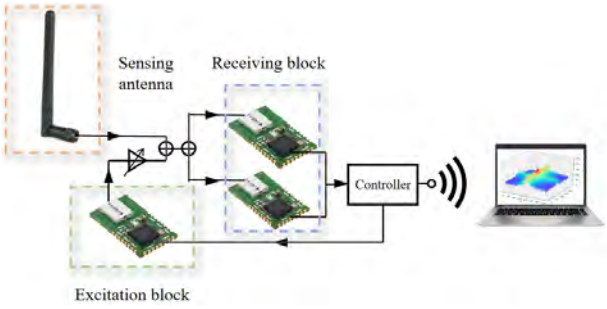

Figure 1: System overview of *WISE*.

for spectrum. S^3 enables sub-Nyquist rate sampling by designing spike-train like filters [23]. However, such customized hardware is not ready for mass production.

We ask the question that, can we enable wideband spectrum monitoring with low-cost, commercial off-the-shelf devices? We have an interesting observation that Ultra-wideband (UWB) technology has the potential to achieve this goal. UWB has a large bandwidth (up to 1GHz), which is originally intended for high-resolution ranging. The time-of-flight (ToF) information is derived from the channel impulse response (CIR). The key point is that the CIRs not only present the channel information between the UWB TX and RX pair, but also record all in-band ongoing transmission in the air. It brings the feasibility that we can obtain wideband channel information from UWB receivers. UWB technology has already been integrated into commercial products, such as smartphones (e.g., iPhone 11/12 Pro [3, 43], Galaxy Note 20 Ultra [37], and Xiaomi MIX 4 [45]) and IoT devices (e.g., Air tag [1], Apple watch [4] and Samsung Galaxy SmartTag+ [41]), which indicates that these daily devices may be turned into a spectrum sensor that facilitates the large-scale spectrum sensing.

In this paper, we present *WISE*, a low-cost WIdeband Spectrum sEnsing unit. As Figure 1 shows, in *WISE*, there is an excitation block, a receiving block, and a sensing antenna. The excitation block transmits UWB packets continuously to trigger the receiving block. These UWB packets and in-air signals from the sensing antenna are combined and then fed into the receiving block. CIRs are extracted from the receiving block, from which we can derive the frequency and bandwidth of the in-air signals. Although the idea sounds straightforward, it is not trivial to achieve the goal. Since the low-cost UWB devices can not afford high-speed clocks and ADCs to support high sampling rates and high data transfer rates, they show some inherent limitations, including low SPI speed and low accuracy. To make things complicated, it is hard to predict the power level of external signals. We attempt to overcome these challenges as follows:

Low accuracy. A spectrum sensor with UWB chips needs to provide accurate and reliable sensing results. However, due to the low-cost nature of UWB technology, we can hardly ensure that the hardware returns reliable results. Since these chips are proprietary technology, we do not have access to the internal designs. Thus, it is hard to analyze their working mechanism but can only observe their responses to external stimuli. From our experiments, we observe that DW1000, a popular UWB chip on the market, may return noisy CIRs which can lead to poor sensitivity and false positives for channel occupation. Even for the same stimulus, two DW1000 chips will return different CIRs, each with some spurious energy at random frequencies. To address this challenge, we design a mechanism to extract in-air signals from the noisy UWB CIRs, separating external in-air signals from internal UWB signals. To handle the spurious and random frequency response, in *WISE*, we utilize two UWB receivers and let them work in parallel. Since the two chips are unlikely to generate the same spurious frequency response, by taking the intersections from the two receivers, spurious frequency responses can be eliminated.

Low SPI speed. Limited by the SPI speed (20Mbps at maximum), it takes almost 2ms to fetch one CIR sample (1016 points) from the UWB device, i.e., DW1000. *WISE* will miss fleeting signals, such as radar signals, that appear when the chip is performing SPI communication. To address this challenge, instead of getting a complete CIR sample, *WISE* will just get a portion of the CIR. This will reduce the time required for SPI communication but comes at the sacrifice of frequency resolution. We design a mechanism to detect channel occupancy with incomplete CIR samples. We also carefully decide the inter-packet time interval so that *WISE* has a high probability to detect radar signals.

Non-predictable signal power. When a high power base station or Access Point is in close proximity, strong external signals may overwhelm the internal UWB communication, resulting in the receiver failing to detect UWB packets and no CIRs will be available. To make things worse, as the UWB receiver has an automatic gain control unit, it will automatically adjust the receiver gain, which results in uncontrollable scaling of the received signals and makes it hard to estimate the signal power. To address this challenge, *WISE* will dynamically adjust the internal transmission power according to the UWB packet reception ratio. When *WISE* suffers high packet loss, it is possibly due to low SINR. Thus, *WISE* will increase the TX power so that the receiving block has sufficient SINRs to detect UWB packets. As the transmission power of the internal UWB packets is a known system parameter, *WISE* utilizes it as a benchmark to derive the instantaneous AGC gain, and then estimate the actual power of the external signals.

In this paper, we design *WISE*, which is a low-cost wideband spectrum sensor that has high sensing accuracy, good receiver sensitivity, and a wide dynamic range. Different from existing low-cost spectrum sensors [33–35, 47], *WISE* can sense a wide bandwidth with one single detection. *WISE* is implemented with DW1000 UWB chips, which has the maximum receiver bandwidth about 900MHz [14]. *WISE* can detect weak signals down to −85dBm/MHz and has a dynamic range about 60dB. The power estimation error is 3dB. It can also detect transient or fleeting signals like radar. Besides, *WISE* has good ability to detect 5G signals and can accurately estimate the power of 5G signals at different distances and in complex environments. The total cost of *WISE* is about 20 dollars, making it possible to be widely deployed and used for various purposes including 5G base station maintenance, 5G signal propagation research, city-level spectrum planning or interference source localization. As the limitations of DW1000 are generic among UWB devices, the design principles of *WISE* can extend well to other devices.

In this paper, we make the following major contributions:

- We demonstrate the spectrum sensing capability of UWB chips, which provides a new direction to build cheap and wideband spectrum sensors.
- We design *WISE*, a low-cost spectrum sensor that supports up to 900MHz bandwidth with high accuracy, good sensitivity, and wide dynamic range. *WISE* can also detect fleeting radar signals.
- We extensively evaluate the performance of *WISE*. From the results, we can see that *WISE* can achieve good accuracy in busy channel detection and signal power/bandwidth estimation. We also show that *WISE* can detect busy 5G channels and accurately estimate 5G signal power.

The remainder of this paper is organized as follows. In Section 2, we introduce UWB technology and the rationale why UWB can be used for spectrum sensing. We present the system overview in Section 3 and system design details are illustrated in Section 4. Implementation details are described in Section 5 and evaluation results are present in Section 6. We review related works in Section 7 and discuss remaining issues in Section 8. Finally, we conclude this work in Section 9.

2 SPECTRUM SENSING CAPABILITY OF UWB

In this section, we explore the spectrum sensing capability of UWB. We first introduce the UWB technology and then illustrate why it can provide the spectrum sensing function. Following that, we illustrate the system requirements for such a low-cost wideband spectrum sensor.

2.1 Ultra-Wideband Technology

Ultra-wideband (UWB) technology transmits signals over a wide bandwidth (>500 MHz). According to the Federal Communications Commission (FCC), the frequency range of UWB is from 3.1 to 10.6 GHz, and the power spectral density (PSD) limit is −41.3dBm/MHz. Typical applications of UWB include ranging and indoor localization. UWB can track assets at a precision of 10 cm, which is a big advantage over Wi-Fi and Bluetooth. Recently, UWB has been integrated into many commercial devices for positioning, tracking, and sensing. For example, Apple's latest iPhones have enabled UWB technology and Apple also released the UWB-equipped asset tracking gadget, AirTag. Samsung has also launched UWB-enabled smartphones and SmartTag+, which is similar to AirTag.

The key that UWB can achieve high ranging resolution is that it can obtain high-precision timestamps. According to IEEE 802.15.4-2011 standard [27], the LSB of the ranging counter value shall represent 1/128 of a chip time at the mandatory chipping rate of 499.2 MHz, that is, 63.897GHz. DW1000, a popular UWB chip on the market, can provide a time resolution of 15.65 picoseconds.

The frame format of a UWB packet is shown in Figure 2. There is a preamble field, followed by the start of frame delimiter (SFD), PHY header (PHR) and the payload. The UWB TX will record the timestamp when the first symbol of the PHR is transmitted, and accordingly, the RX will record the timestamp when the first symbol of the PHR is received. In this way, time-of-flight (ToF) can be calculated. For the rest of the paper, we will describe our system based on DW1000, a popular UWB chip from Decawave, which has been acquired by Qorvo.

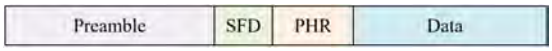

Figure 2: Frame format for UWB packets (from [14]).

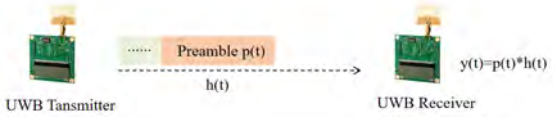

(a) UWB communication

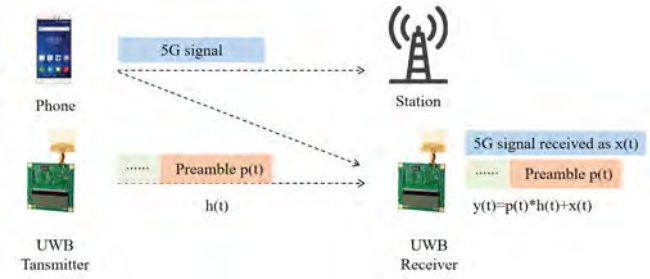

(b) UWB communication with 5G signal

Figure 3: UWB communication with/without in-air signals.

The preamble sequence has a property of perfect periodic autocorrelation, which allows a coherent receiver to determine the exact impulse response of the RF channel between transmitter and receiver [12][14]. DW1000 provides access to the channel impulse response (CIR) data. For each tap of the CIR, it is a complex value, with a 16-bit real integer and a 16-bit imaginary integer. Each tap represents a 1 ns sample interval. To be more precise, it is half a period of the 499.2 MHz fundamental frequency. For simplicity, we say that the sampling frequency is 1 GHz.

2.2 UWB for Spectrum Sensing

Assume that there is only a UWB TX and a UWB RX in the system, as shown in Figure 3(a). When the TX transmits the preamble sequence $p(t)$, the RX will receive

$$y(t) = p(t) * h(t),$$

where $h(t)$ is the channel impulse response (CIR) between the TX and RX, and $*$ denotes convolution. To obtain CIR, the RX performs decorrelation of the received signal $y(t)$ with the known preamble sequence.

When there are other transmitters in the air, as shown in Figure 3(b), we denote the superimposed signals arriving at RX's antenna by $x(t)$. In this case, the RX receives

$$y(t) = p(t) * h(t) + x(t).$$

In this case, the CIR turns out to be:

$$\hat{h}(t) = p(-t) * y(t) = h(t) + p(-t) * x(t). \quad (1)$$

The RX stores $\hat{h}(t)$ in the CIR memory of DW1000. We note that $\hat{h}(t)$ not only contains the information about $h(t)$, but also the other

in-band signals in the air. Transforming Eq. (1) into the frequency domain, it becomes

$$\hat{H}(f) = H(f) + P(f) \cdot X(f). \quad (2)$$

$X(f)$ is the frequency domain representation of the in-air signals, which shows the working frequency and bandwidth of the non-UWB transmitters. $P(f)$ is the frequency domain representation of the preamble sequence.

When the channel between UWB TX and RX is stable, we can consider $H(f)$ as a known constant. Furthermore, according to the measurement result in [13], the UWB signals have a flat frequency response for the whole band (i.e., 500MHz), so we have $|P(f)| \approx c$, where c is a constant. Thus, $\hat{H}(f)$ contains the spectrum usage information, i.e., which frequency bands are occupied and which bands are idle. It indicates that we can use UWB chips for spectrum sensing. Since the bandwidth of UWB is up to 900MHz, we can use the low-cost UWB chip to achieve wideband spectrum sensing. The frequency range of UWB ranges from 3.1GHz to 10.6 GHz, which covers the 3.5 GHz CBRS band and 6GHz unlicensed band. Thus, *WISE* can serve as a spectrum sensor for dynamic spectrum access in these bands.

Here we show some illustrative experiment results. We set up a USRP next to the UWB transceivers to transmit single-tone signals at 3.964GHz. We read CIR samples from DW1000 and perform FFT on the samples to get the channel frequency response (CFR). As the CIR sampling interval is 1ns and there are 1016 samples in total, the frequency resolution of the FFT bins is roughly 1MHz. Figure 5(a) shows the CFR when the USRP is not transmitting and Figure 5(b) shows the CFR when the USRP is transmitting. From Figure 5(b), we can see that the CFR has high peaks around 3.964GHz, which indicates that the UWB captures the single-tone signal transmitted by the USRP. This demonstrates the feasibility of using UWB for spectrum sensing.

2.3 System requirements

As UWB is low-cost and wideband by nature, when using it as a spectrum sensor, it needs to meet the following performance requirements:

- High accuracy: It should provide reliable results for channel occupancy detection, with low false positive rate and low false negative rate for the entire band; it should also provide accurate estimations of the signal power/bandwidth.
- Good sensitivity: First, it should be able to detect weak signals. We expect that *WISE* should have the same sensitivity as a typical software-defined radio, e.g., USRP. Second, it should be able to detect short transient packets and fleeting signals, such as radar signals in CBRS band.
- Wide dynamic range: It reflects the ability of *WISE* to detect both high-power and low-power signals. It should be able to detect both strong and weak signals.

In the following sections, we will describe how we design *WISE* to meet these requirements.

3 *WISE* OVERVIEW

In this section, we first present the system structure and then give the signal processing flow of *WISE*. As shown in Figure 1, *WISE* has three main components, the excitation block, the receiving block and the controller. The excitation block is a UWB transmitter, which is responsible for transmitting UWB packets continuously. These packets serve as excitation signals to trigger the receiving block. The receiving block consists of UWB receivers, which are responsible for retrieving the CIRs. The sensing antenna is used for picking up ongoing transmissions in the air. A combiner combines the sensing antenna and excitation signals, and the output from the combiner is fed to the receiving block via a cable. This is to guarantee that the channel between the UWB TX and RX is as stable as possible. Note that the signals from the excitation block are not emitted into the air, so its continuous transmission will not cause long-lasting interference. The controller is responsible for TX power control, working mode selection and CIR processing.

Figure 4 shows the signal processing flow in *WISE*. Data processing is mainly performed at the receiving block and it supports two working modes. In normal mode, the first step is to extract in-air signals from noisy CIRs. It is essential to separate the internal UWB signals and in-air signals, which greatly reduces noise level and improves the system sensitivity. The second step is to estimate the power of signals. *WISE* uses the internal signal as the benchmark to estimate the instantaneous AGC gain and then estimates the power of external signals. Then, we use a dynamic threshold to classify busy/idle channels. The last step is to improve the frequency resolution. The idea is to concatenate multiple CIRs to generate a longer observing window and thus achieve finer frequency resolution. The signal processing flow in radar mode is similar, but differs in the way that we perform in-air signal extraction and power estimation. It also does not have the CIR concatenation step. The details can be found in Section 4.

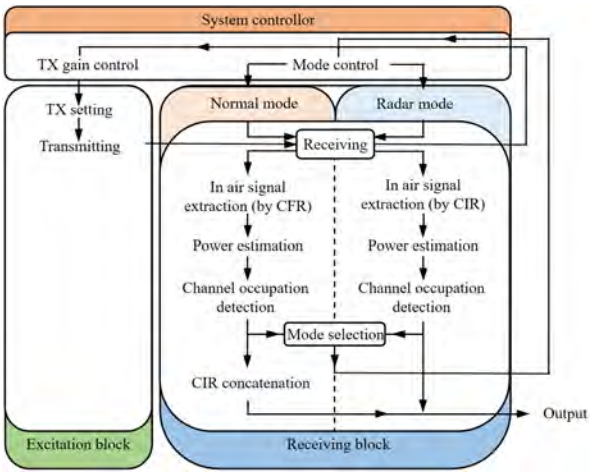

Figure 4: Signal processing flow in *WISE*.

4 *WISE* DESIGN

In this section, we present the design details for each component in *WISE*.

4.1 Excitation Block

The excitation block is a UWB transmitter, which is intended to trigger the receiving block. According to the user manual of DW1000 [14], once the preamble sequence is detected, the receiver will begin accumulating correlated preamble symbols. Thus, the excitation block transmits UWB packets continuously, which will trigger the receiving block to get constantly updated CIRs. In *WISE*, we use UWB transceivers just for obtaining CIRs, not for data communications. Thus, we put only 1 byte data in the payload to make the packets as short as possible.

In order to make sure that the preamble signal can be detected by receivers so as to trigger spectrum sensing, the excitation block needs to dynamically adjust the transmission power to avoid the UWB preamble being buried in strong external signals or being too strong to bury the external signals. Besides, we hope *WISE* can have good sensitivity and wide dynamic range. In *WISE*, we adopt the following control strategy. In the excitation block, we switch the TX power level between two states. By default, the excitation block will transmit at a low power level (State 1). When no UWB packets are detected by the receiving block for a certain time interval, which is possibly due to low SINR, the receiving block will raise a timeout event. In this case, *WISE* will increase the transmission power of the excitation block (State 2). When the high-power external signal vanishes, *WISE* will switch the TX power to the default low level (State 1).

In order to determine these two power levels, we first use an attenuator to tune the power level of the excitation block. The results are shown in Figure 16. We can see when with a weak preamble power (i.e., −104.3 dBm/MHz), the channel impulse response is very noisy, which makes it hard to extract in-air signal and results in a narrow sensing range. Therefore, we attempt to increase the preamble power. When the power level comes to −86.3 dBm/MHz, *WISE* has the widest sensing range and also has good sensitivity. Thus, we set the power level to be −86.3 dBm/MHz in State 1. As DW1000 can adjust the transmission power around 30 dB and we want to have a wide dynamic range, we set the power level to be −56.3 dBm/MHz in State 2.

Through testing, we find that *WISE* have around 30dB dynamic range in one state. That is, it can detect signals from −85dBm/MHz to −54 dBm/MHz in State 1, and in State 2, it can detect signals with power from −60dBm/MHz to −34dBm/MHz. The whole dynamic range is −85 dBm/MHz ∼ −34dBm/MHz.

4.2 Receiving Block

Before introducing the design details of receiving block, we first present how UWB chips estimate channel impulse response, which will help readers understand the design rationale of *WISE*.

4.2.1 CIRs from UWB. According to IEEE standard, each preamble symbol is about 1us and the number of symbols in the preamble can range from 64 to 4096. DW1000 obtains CIR by cross-correlating the received signals with the predefined preamble sequence. The accumulation results are stored in a buffer, named accumulator. Accumulation stops when detecting SFD, while it may stop earlier if the accumulator grows quickly. After saturation, channel impulse response, i.e., the accumulation results, could be read from the accumulator buffer.

As the values we get from the accumulator buffer are the CIR, to analyze the frequency response, we perform FFT on the CIR to get the CFR.

4.2.2 In-air Signal Extraction. According to Equation (2), the CFR we obtained is actually $\hat{H}(f)$, while the spectrum occupation information is contained in $X(f)$. $H(f)$ is the channel response corresponding to the wired channel between UWB TX and RX, which is supposed to be stable. Figure 5(a) shows the CFR when there is no external signal. As long as *WISE* is set up, we can consider $H(f)$ to be constant. During initialization, *WISE* will turn off the RF antenna, where there are only internal UWB signals via the wired cable. *WISE* can obtain $H(f)$ under this circumstance and use it for the following signal extraction procedure. Thus, we can measure $H(f)$ as a system parameter and subtract it from $\hat{H}(f)$. $P(f)$ is the frequency response of the preamble sequence. As defined in IEEE 802.15.4-2011, the preamble is a sequence of short pulses. From the measurement results in [13], we can see that UWB signals have a flat frequency response for the whole band. Thus, we have $|P(f)| \approx c$, where c depends on the transmission power of the excitation block and is also a known system parameter.

However, we can not directly apply Equation (2) to estimate $X(f)$. This is because DW1000 has an automatic gain control (AGC) unit. The AGC will dynamically adjust the receiver gain to ensure optimal receiver performance. Assume that the actual amplitude for frequency f is a_f while the amplitude of frequency f in the FFT results is A_f, then the receiving amplitude $A_f = ka_f$, where k is an unknown coefficient. So the $\hat{H}(f)$ is actually described by Equation (3):

$$\hat{H}(f) = k \cdot [H(f) + P(f) \cdot X(f)] . \tag{3}$$

Therefore, we need to figure out k before estimating $X(f)$.

We use a signal generator to transmit 50MHz and 300MHz signals and the corresponding CFRs are shown in Figure 6. Comparing with Figure 5(a), where there is no in-air signals and thus only the $k \cdot H(f)$ component, the $P(f) \cdot X(f)$ term has more spikes in the frequency domain. Thus, we can use a low-degree polynomial to fit the more smooth $k \cdot H(f)$ part, shown as the red curve in Figure 6. We apply a 16-order polynomial curve-fitting on $\hat{H}(f)$. We denote the fitting results by $F(f)$, which is mainly dominated by $k \cdot H(f)$. As we mentioned above, $H(f)$ is a known system parameter. Then, we model it as an optimization problem to determine the scaling factor k as follows:

$$k = \arg\min_{\alpha} \sum_{f=f_{\min}}^{f_{\max}} [F(f) - \alpha \cdot H(f)]^2 . \tag{4}$$

In this paper, we simply iterate over the possible range of k and determine the optimal value. Since the scaling factor k is now known, we can estimate $X(f)$ as follows:

$$|X(f)| = \frac{\left|\frac{1}{k} \cdot \hat{H}(f) - H(f)\right|}{|P(f)|}.$$

Comparing Figure 5(c) and Figure 5(d), we can see that with AGC calibration, the extracted in-air signal has a better SNR.

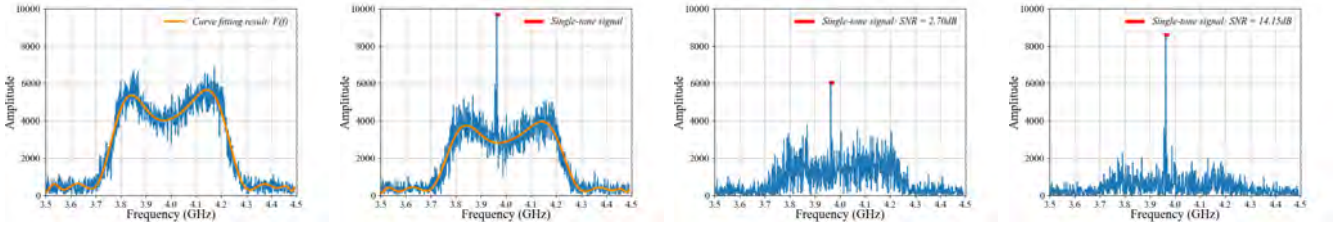

(a) CFR without external signal (b) CFR with external signal (c) Without AGC calibration (d) With AGC calibration

Figure 5: CFRs with and without external signals.

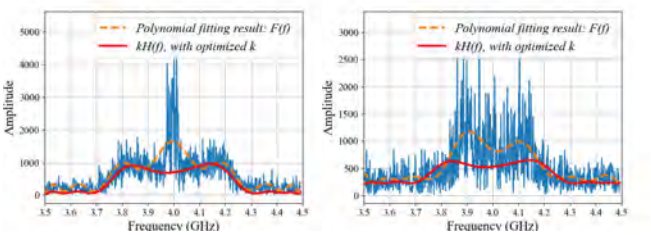

(a) 50MHz signal (b) 300MHz signal

Figure 6: CFRs for 50MHz and 300MHz signal.

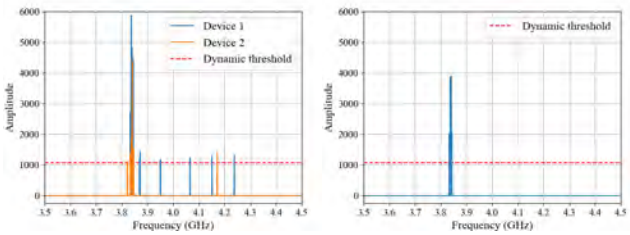

(a) CFRs from Device 1 and Device 2 (b) Intersections of Device 1 and Device 2

Figure 7: Spurious frequency response.

4.2.3 Signal Power Estimation. From the above step, we have extracted the in-air signal from the CFR. Next, we estimate the signal power for each frequency bin. According to the user manual of DW1000, the power of every frequency bin can be calculated using the following equation:

$$Power_{Rx}(f) = 10 \times \log_{10}\left(\frac{A_f^2}{N^2}\right) - C \text{ dBm}. \quad (5)$$

Here, A_f is the amplitude of frequency f in $X(f)$ and N is the number of preamble symbols involved in the accumulation process, which can be read from PACC register. C is a constant for calibration, which is defined as 121.74 according to the DW1000 user manual. Since AGC has amplified/attenuated the receiving signals by the scaling factor k, the Equation (5) turns to be:

$$Power_{Rx}(f) = 10 \times \log_{10}\left(\frac{A_f^2}{k^2 \cdot N^2}\right) - C \text{ dBm}.$$

Thus, we can estimate the power for each frequency bin in the CFR.

4.2.4 Channel Occupation Detection. In order to determine whether the channel is occupied, we attempt to set a dynamic threshold. We design this threshold as follows:

$$Threshold = \beta \cdot mean(|X(f)|) \cdot \frac{\sum_f |X(f)|}{max(|X(f)|)}, \quad (6)$$

where β is a coefficient. For a frequency bin, if its amplitude is larger than the threshold, we consider that the channel is occupied; otherwise, we consider the channel to be idle.

Besides, we observe that the UWB chips may have some spurious frequency responses. We observe that, if we feed the same stimulus to the UWB chip multiple times, the chip may return different frequency responses; if the same stimulus is fed into two chips at the same time, they may also return different results, as shown in Figure 7. A nearby transmitter is transiting at 3.84GHz, but both devices have some spurious peaks at other frequencies. This phenomenon is quite random and unpredictable. As UWB is proprietary technology, it is hard to find the root cause for this uncontrollable phenomenon. In order to address this problem, *WISE* integrates two UWB receivers in the receiving block. It is very unlikely that the spurious responses will appear at the same frequency. Thus, by taking the intersection of the CFRs from the two receivers, these spurious responses can be eliminated. By taking the intersections of Device 1 and Device 2 in Figure 7(a) , the spurious responses are eliminated. The results are shown in Figure 7(b). We will show in Section 6.2. that with two receivers the false positive rates can be greatly reduced.

Through the above steps, we can determine the frequency, power and bandwidth of the in-air signal.

4.2.5 Radar Mode. As we mentioned in Section 4.2.1, *WISE* senses the in-air signals within the duration of the preamble. For a 64-symbol preamble, the preamble lasts for 64µs. However, because of the limit of SPI speed (e.g., 20Mbps at maximum), it takes almost 2ms to fetch the 1016-point CIR data from the DW1000 chips. That means that *WISE* can only perform one round of spectrum sensing in every 2ms, during which the 64µs is the sensing time while the rest time is for SPI communication. The long SPI reading time

leads to a high possibility of missing fleeting or transient signals. For example, some radar signals have only one short pulse (e.g., 1−100µs) every 1ms. Thus, it is difficult to detect those signals, as the pulse has a high probability to occur when the *WISE* is performing SPI communication.

To address this problem, we define a radar mode in *WISE*. As more CIR points means longer SPI communication time, in radar mode, instead of getting 1016-point CIR, we just read a portion of each CIR sample from the DW1000 chip. On one hand, in radar mode, we aim to have a high update rate and thus prefer as few CIR points as possible; on the other hand, *WISE* wants to preserve a good frequency resolution. Given the 1ns sampling interval, in order to have at least 10MHz frequency resolution, we need at least 128 CIR points for FFT operations. Hence, *WISE* retrieves 150 CIR points in radar mode (extra 22 points for rough AGC calibration as explained below). According to the user manual, DW1000 arranges the CIR buffer so that the first path index is around 750. Thus, we will read the CIR indexing from 615 to 765, reducing the SPI communication time to around 500µs. However, it comes at the sacrifice of information and spectral resolution.

In this mode, the procedure for in-air signal extraction in Section 4.2.2 no longer works well due to poor resolution. Thus, we propose an alternative solution for in-air signal extraction and signal power estimation. We further separate the 150-point CIR into two parts. The first part contains CIR1=CIR[615:735] and the second part contains CIR2=CIR[735:765]. We mainly use CIR1 for signal detection and CIR2 for power estimation.

As we mentioned above, the first path index is around 750. In *WISE*, the first path refers to the wired channel between the excitation block and the receiving block, i.e., $H(f)$. Thus, the energy of CIR2 mainly corresponds to the UWB signal received via the wired channel, i.e., the $k \cdot H(f)$ term in Equation (3). As the transmission power $Power_{TX}$ is a known system parameter, we can estimate k as follows:

$$k \approx \frac{\sum_{i=735}^{765} CIR[i]^2}{Power_{TX}}.$$

Compared with CIR2, the first path is less dominate in CIR1. Thus, for signal detection, we pad zeros to CIR1 and perform 128-point FFT on CIR1 to get the CFR. We also use Equation (6) to detect the channel occupation.

Although we have reduced the SPI communication time, there is still around 500µs interval between two detections. There are possibilities that radar pulses will appear in this time gap and results in miss detection. As radar signals are composed of a number of pulses, we can detect its existence as long as one of the pulses falls within the UWB preamble duration.

We can formulate the problem for radar detection as follows. Assume that the radar signal has a pulse lasting for r second and one pulse is transmitted every R second. We use $x(t)$ to denote the radar pulse occurring at time t. There are K pulses in total. We use $Radar(t)$ to denote the radar signal:

$$Radar(t) = \begin{cases} x(t) & R \cdot k < t < R \cdot k + r, \quad k = 0, 1, \cdots, K-1 \\ 0 & else \end{cases} \tag{7}$$

We assume that the UWB preamble lasts for μ second. We can use a binary function to indicate whether *WISE* is sensing or not:

$$WISE(t) = \begin{cases} 1 & T \cdot m + \delta < t < T \cdot m + \delta + \mu, m = -\infty, \cdots, 0, \cdots, \infty \\ 0 & else \end{cases} \tag{8}$$

where T is the sensing cycle of *WISE* and δ is the time offset between the *WISE* and radar cycles. When *WISE* is sensing at time t, $WISE(t) = 1$; otherwise, *WISE* is performing SPI communication and $WISE(t) = 0$. Note that we set $t = 0$ when the first pulse in the radar signal is transmitted, and thus in Equation (8), m could be negative.

In order to detect the radar signal, we need to gurantee that at least one of the pulses is transmitted when *WISE* is sensing, that is, we need to gurantee that for any $\delta \in [0, T]$, the following condition holds:

$$\sum_t Radar(t) \cdot WISE(t) > 0. \tag{9}$$

We need to determine the appropriate *WISE* sensing cycle T. To make things simple, we can search for a feasible T, starting from the minimum value 564μs (e.g., 64μs for sensing, 500μs for SPI communication).

Figure 8 gives an illustrative example. Consider a typical radar signal, where R = 1ms, r = 1µs, k = 15. Assume that the preamble of UWB packet lasts for 64μs, i.e., μ = 64μs. When T = 579μs (e.g., 15μs idle time), Equation (9) holds for any δ. By setting the inter-packet time to 15μs, we can guarantee that *WISE* can capture at least one radar pulse. Here, we simply assume that the inter-packet interval is a constant value. In future work, we can set a variable inter-packet interval.

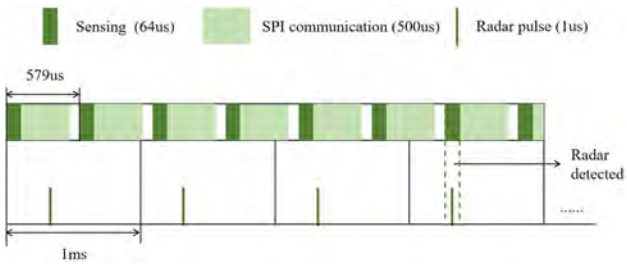

Figure 8: Setting inter-packet interval for radar detection

As we mentioned above, we reduce the SPI communication time at the sacrifice of resolution. Thus, *WISE* will switch between two modes, i.e., the normal mode and the radar mode. To avoid missing radar signals, by default, *WISE* will stay in the radar mode; it will switch to the normal mode when detecting a lasting signal, as the normal mode can provide better resolution and higher detection accuracy. By comparing the CFRs from two scans, we can determine the signal is lasting or fleeting. The working flow of *WISE* is shown in Figure 9.

4.2.6 Packet Aggregation. As we mentioned above, the CIR sampling interval is 1ns and there are 1016 samples in total. Thus, the frequency resolution of the FFT bins is roughly 1MHz. This may result in inaccurate bandwidth estimation and miss some narrowband signals. In order to have a finer frequency resolution, we perform

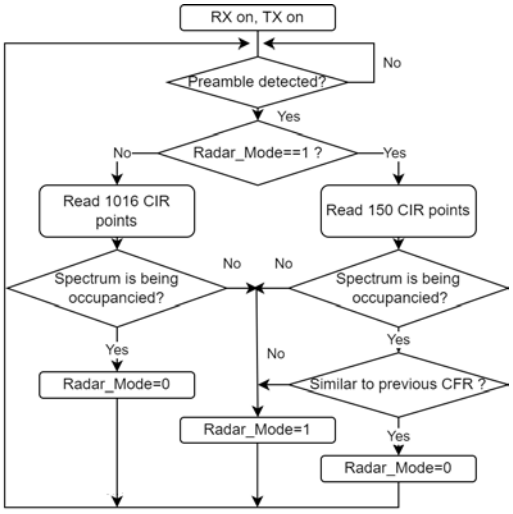

Figure 9: Mode selection in *WISE*.

packet aggregation on successive packets. The idea sounds straightforward. By concatenating CIRs from successive packets, we can get a longer observation window. Then, we will naturally have a finer frequency resolution.

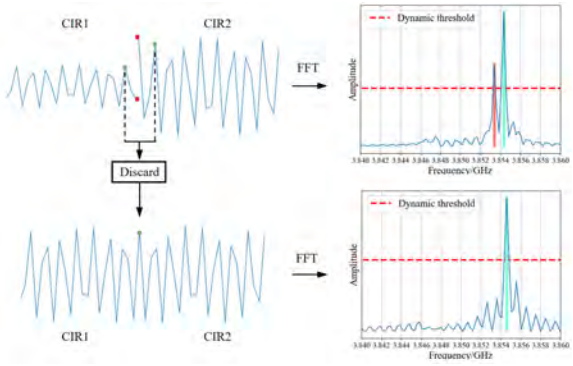

Figure 10: CIR concatenation.

Here, we convert the CFRs (after noise reduction) to the time domain CIRs by IFFT. Figure 10 shows the CIRs for 2 successive packets. We can see that these CIRs are not continuous in the time domain. Direct concatenation will lead to spectral leakage, where the FFT results are also shown in Figure 10.

In order to address this issue, we do not directly concatenate CIRs, but align successive CIRs according to the following steps.

First, we normalize the amplitude of CIRs, so as to avoid the data discontinuity caused by large amplitude differences. Second, in order to minimize data discontinuity, we need to find a data sample in the two CIRs that have the same data value and first derivative. To make the computation easy, we identify the last peak in the preceding CIR and the first peak in the current CIR. We discard the CIR points between the two peaks and concatenate the two CIRs (by replacing the two peaks with their average value). This

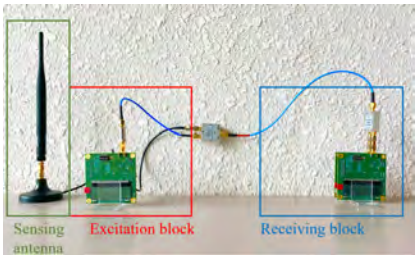

Figure 11: *WISE* prototype

is reasonable for two reasons. First, after amplitude normalization, peaks have the same values; second, the first derivative of peaks are both zeros. Thus, concatenating two peaks can provide good data continuity and avoid frequency leakage. Figure 10 illustrates this process. In this way, the concatenated CIRs turn out to be a continuous signal. We can see that after CIR alignments, the spectral leakage phenomenon has been greatly improved.

To improve the spectrum update rate under concatenating, in *WISE*, we build a queue to store N successive CIRs. When *WISE* obtains a new CIR, *WISE* will delete the oldest CIR and appends the latest CIR to the queue. Finally, *WISE* performs packet aggregation on these N CIRs. In this way, the spectrum sensing results can be updated every time when a new CIR is obtained.

5 IMPLEMENTATION

5.1 Prototype

We build a prototype of *WISE* with three DW1000 UWB chips (EVK1000 [15]), one for the excitation block and two for the receiving block. DW1000 supports 6 RF bands from 3.5GHz to 6.5GHz and the maximum receiver bandwidth is about 900MHz. In this work, the main goal is to demonstrate the feasibility of UWB chips for spectrum sensing, and thus we use a laptop to serve as the controller, which can be easily replaced by Raspberry Pi or MCU. Two Cheetah SPI host adapters serve to connect the EVK1000 to the USB port of the laptop, which can provide 20Mbps SPI speed. The communication between the controller and DW1000 is performed via the SPI interface. Figure 11 gives a picture of the prototype we have built.

We control the EVK1000s by the *decadrivers* provided by Decawave. For the excitation block, we adopt the following configuration: 64-symbol preamble, 64MHz PRF, 6.8MHz data rate and 1 byte payload. We use *Transmit Power Control* register to dynamically control the TX gain. We control the *System Control* register to trigger packet transmission. The receiver will read either 150 or 1016 points CIR from the *ACCMEM* register, depending on the working mode of *WISE*.

On the controller, we use python to process the CIR data. We use *fft* and *ifft* functions from *scipy* for transformation between CIR and CFR, and use *polyfit* function from *numpy* for 16-order polynomial curve fitting. As most processing procedures are simple operations, the processing latency is low. The controller will decide the TX gain and working mode for the next detection based on the processing result.

5.2 Testbed

We evaluate the performance of *WISE* through a group of experiments. We test *WISE* under two different settings. In the first setting, we use a signal generator to generate controlled signals. Here we use Keysight M8190A arbitrary waveform generator [28]. We use SystemVue [30], a software produced by Keysight, to configure the parameter of signals and download the designated signals into M8190A. Then, the output from M8190A is connected to the Keysight E8267D PSG Vector Signal Generator [29], which will upconvert the baseband signal to any frequency between 250kHz and 20GHz. Finally, the signals with designated frequency, bandwidth, and power are generated. In the second setting, we use *WISE* to monitor on-going 5G signal in the air. We use a XIAOMI 12 pro 5G to download a large file from the Internet and use Speedtest to get the connection information, including channel frequency, signal bandwidth and power. We put the *WISE* prototype 2 meters away from the 5G smartphone, as shown in Figure 20. The information from Speedtest serves as the ground truth.

6 EVALUATION

In this section, we present the evaluation results of *WISE*. We mainly consider the following evaluation metrics:

- False Negative Rate (FNR) : The proportion of occupied frequencies that *WISE* incorrectly reports as empty.
- False Positive Rate (FPR): The proportion of empty frequencies that *WISE* incorrectly reports as occupied.
- True Positive Rate (TPR): the proportion of occupied frequencies that *WISE* correctly reports as occupied.

6.1 Frequency Response

We measure the frequency response of *WISE*. DW1000 supports 6 channels, where channel 1, 2, 3 and 5 have 499.2MHz bandwidth, while channel 4 and 7 support above 1GHz bandwidth (according to the datasheet, the maximum receiver bandwidth is approximately 900 MHz). Here, we choose to measure the frequency response of channel 2 and 7, as there are no ambient signals at these two bands and thus we can get accurate frequency responses. We believe that the measurement results are representative of other channels. Channel 2 covers from 3.774GHz to 4.243GHz, and channel 7 covers from 5.980GHz to 6.999GHz. In this experiment, to measure the frequency response, we use the signal generator to generate a 1MHz BPSK signal at −70dBm. We sweep its frequency from 3.7GHz to 4.3GHz when measuring the frequency response of channel 2, and sweep the frequency from 6.04GHz to 6.94GHz when measuring channel 7. Both channels are measured with 1MHz frequency resolution. In order to avoid signal attenuation over wireless channels, in this experiment, the output from the signal generator is connected to *WISE* input port via a wire.

Results are shown in Figure 12. The actual bandwidth of channel 2 is approximately 400MHz, covering from 3.8GHz–4.2GHz. The best frequency range for channel 7 to detect signals is from 6.14GHz to 6.84GHz. Generally speaking, *WISE* has a flat frequency response; for channel 2, the available bandwidth is about 400MHz, while for channel 7, the available bandwidth is about 700 − 900MHz.

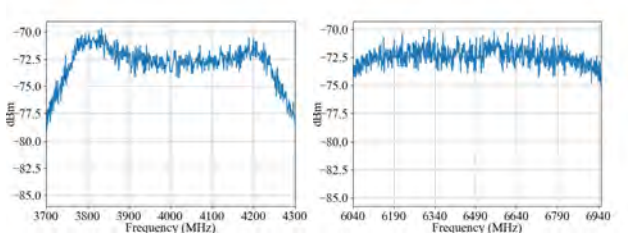

(a) Channel 2 (b) Channel 7

Figure 12: Frequency response of channel 2 and channel 7.

6.2 Different Modulation Schemes

To avoid interference from ambient cellular or ISM band signal, we configure the working channel of DW1000 to be channel 2, ranging from 3.774 GHz to 4.243 GHz. We check with a spectrum analyzer that the band is originally idle. We test with three different kinds of modulation schemes, i.e., BPSK, QAM and OFDM. The signal bandwidth is 10MHz. We tune the center of signal frequency from 3.8 GHz to 4.2 GHz, at 20MHz interval, which results in 21 channels. At each channel, we transmit the designated signals for 400 times. At a specific frequency f, if the signal is missed, we count it as a false negative event; if other frequencies (f') are identified to be occupied, we count it as a false positive event at f'.

Results are shown in Figure 13. In Figure 13(a), we show FPR and FNR for different frequency bands. In each frequency, we will transmit the signals for 1200 times in total (400 times for each modulation scheme), and obtain the FNR by dividing the count of false negative events by total transmission times. We can obtain FPR similarly. In all cases, the FPR and FNR are lower than 1%, and for more than 75% of the bands, the FPR/FNR is lower than 0.1%/0.3%, respectively. We note that FNR is generally higher than FPR. This is because FN event happens when a signal is missed at frequency f, while FP event can happen at any frequency other than f. In Figure 13(b) and Figure 13(c), the horizontal axis represents different modulations. Each designated signal will be transmitted for 8400 times in total (400 times for each channel). Figure 13(b) and Figure 13(c) show that using two receivers can reduce FPR by 10 times, which is a great improvement compared to the single receiver. We can see that *WISE* has indistinguishable performance for different modulation schemes, as the difference of FNR and FPR between different modulation schemes is less than 0.1% when two receivers have been used.

Also, we compare the performance of *WISE* with different spectrum sensing methods, including Sweep-Sense [24], S^3 [23], and Big-band [26]. Results are as shown in Table 1. From Table 1, we learn that, *WISE* has similar performance to S^3. However, the spike-train of filters in S^3 is customized hardware, which is not ready for mass production. Nevertheless, *WISE* is built with commercial devices.

6.3 Different Levels of Spectrum Occupancy

In Section 6.3, we evaluate the performance of *WISE* under different levels of spectrum occupancy. We divide the whole band (i.e., 3.8

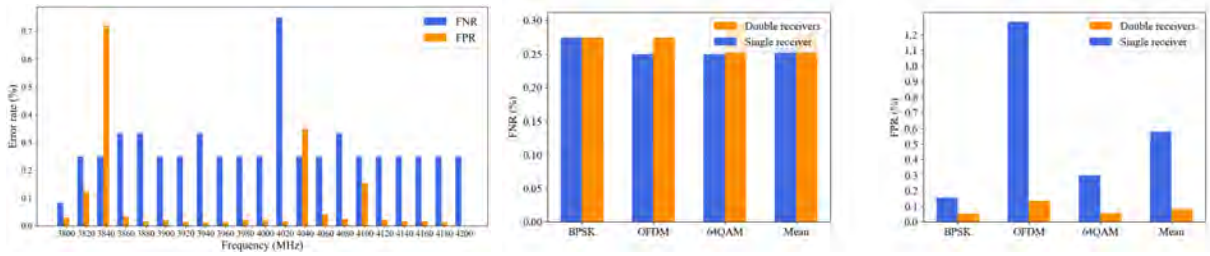

(a) The performance at different frequencies (b) FNR of modulation schemes (c) FPR of modulation schemes

Figure 13: *WISE* performance under different frequencies and modulation schemes.

Table 1: Sum of false positive rate and false negative rate for *WISE* and state-of-the-art prior work

Modulation	Bigband	SweepSense	S^3	*WISE*
BPSK	14.38%	4.88%	0.00%	0.28%
64QAM				0.35%
OFDM				0.35%

GHz-4.2 GHz) into 20 channels, each with 20 MHz bandwidth. In SystemVue, we emulate 20 transmitters, one at each band, each with 20MHz bandwidth. We change the level of spectrum occupancy by switching the transmitters on and off. We vary the spectrum occupancy from 10% to 90%. Under each level of spectrum occupancy, we randomly select six combinations of transmitters. For example, if 10% of the spectrum is busy, which corresponds to 2 active transmitters, we will randomly select six combinations out of the total 190 possible combinations. For each spectrum occupancy and transmitter combination, we will transmit signals for 400 times. If the signal in the positive band is missed, we count it as a false negative event; if other empty bands are identified to be occupied, we count those events as false positive events. Then we can obtain the FNR/FPR by dividing the count of false negative events/false positive events with total 400 transmissions in each spectrum occupancy level.

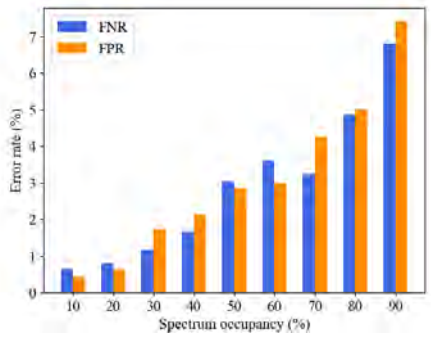

Figure 14: CFRs under different levels of spectrum occupancy.

Results are shown in Figure 16. We can see that *WISE* has good performance at different levels of spectrum occupancy. When the spectrum occupancy is below 40%, the FPR/FNR is less than 2%; when the level of spectrum occupancy is below 80%, the FNR and FPR are less than 5%. However, when the level of spectrum occupancy increases, the performance of *WISE* will get worse. When spectrum occupancy is up to 90%, the FNR and FPR will be around 7%. By comparing the CFR under different levels of spectrum occupancy, we infer that, when the spectrum is densely occupied, the high FNR/FPR is caused by the low power spectral density. As the signal is generated by M8190A, given the limited transmission power, the power spectrum density decreases when the bandwidth increases. This is the problem of the signal generator, but not *WISE*. We believe that the performance of *WISE* may not degrade when the spectrum is occupied by independent transmitters.

6.4 Bandwidth Estimation

In this experiment, we use the testbed to generate BPSK signal at the center frequency of 4GHz, and change its bandwidth from 50MHz to 800MHz at 50MHz granularity (e.g., 50MHz, 100MHz, 150MHz, $\cdots$). We configure the DW1000 to work at channel 7 (maximal 900MHz bandwidth). Under each bandwidth setting, we repeat the experiment for 500 times. Thus, we can get 500 CIRs for each bandwidth. We use those CIRs to evaluate the performance of bandwidth estimation when concatenating different numbers of CIRs (e.g., 1, 4, 8, 16).

Results are shown in Figure 15. We find that, without CIR concatenation, the maximum bandwidth that *WISE* can detect is 300MHz; when the signal bandwidth is larger than 300MHz, there will be huge errors in bandwidth estimation. However, when we concatenate 4 CIRs, the bandwidth estimation will be more accurate, unless the bandwidth of the testing signal is larger than 400MHz. We can get better performance by concatenating more CIRs. However, when we concatenate too many CIRs, the marginal gain decreases and performance will not have much improvement, but will consume more computing resources. We find that 4 CIRs aggregation is the best choice by trading off between performance and computing resource consumption. We can accurately estimate the signal whose bandwidth is below 400MHz. We believe that it can satisfy the application requirements as there are hardly any signal has such large bandwidth in sub-6G.

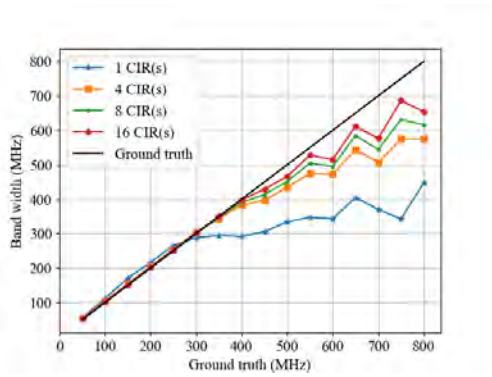

Figure 15: The performance of bandwidth estimation with packet aggregation.

6.5 Sensitivity under different levels of UWB power

In this experiment, in order to avoid signal power attenuation over wireless channels, the output from the signal generator is connected to *WISE* input port via a wire. we configure DW1000 to work at channel 2. We use the signal generator to transmit a 10 MHz BPSK signal at 3.96 GHz. We set the center frequency to be 3.96 GHz as it is the least sensitive frequency according to the frequency response curve of channel 2. Then, we adjust its transmission power from −85 dBm to −20 dBm with 5 dBm interval. In each power level, the signal will be transmitted for 100 times. We evaluate the signal power level that *WISE* can detect under different UWB TX power settings. If *WISE* truly detects the signal, we will count it as a true positive event. Then we can calculate the detection rate by dividing the count of true positive events by the total 100 transmissions.

The result is shown in Figure 16. When we set UWB TX power to −86.3dBm/MHz (State 1), *WISE* is able to detect signals whose power is from −85dBm/MHz to −54dBm/MHz, and the detection rate is 95% at −85dBm/MHz; when we increase the UWB power to −56.3dBm/MHz (State 2), the valid power range is −60dBm/MHz ∼ −34dBm/MHz. Therefore, the total power range that *WISE* can detect ranges from −85dBm/MHz to −34dBm/MHz. Obviously, *WISE* has better sensitivity when the UWB TX power is low. In order to find out the weakest signal that *WISE* can detect, we set the TX power of the excitation block to −104.3dBm/MHz (by adding an extra 20dB attenuator), which is the minimum power that UWB can receive. In this case, *WISE* can detect the BPSK signal at −89dBm/MHz with 98% detection rate. Therefore, if we set the UWB power to −104.3dBm/MHz, *WISE* can detect −89dBm/MHz weak signals. This sensitivity is better than Sweepsense [24] and is equivalent to USRP N210.

6.6 Power Estimation

From the frequency response curve, we notice that the response are diverse at different frequencies. To avoid distortion in power estimation, we have calibrated the result according to the frequency response curve. In this experiment, to see whether the calibration works, we test with signals at different frequencies. We use the signal generator to generate a 50MHz BPSK signal at 3.9GHz, 4.0GHz, 4.1GHz and adjust its power from −85dBm to −35dBm, where the UWB TX power is set to −86.3dBm/MHz. Note that in Section 6.5, the bandwidth of the testing signal is 10MHz, while the bandwidth is 50MHz in this experiment.

Results are shown in Figure 17. *WISE* can estimate the signal power within ±3dB error in its working range. Here we find that although the signal power exceeds −44dBm, it is still able to detect the signal. This is because we use a 50MHz signal, and its power density is lower than a 10MHz signal given the same total power. We can see that *WISE* has good accuracy in estimating signal power.

6.7 Radar Detection

we evaluate the performance of *WISE* in detecting radar signals. According to DeepRadar [38], we test with different types of radar signals in the CBRS band. We change the parameters of radar signals, including the pulse repetition rate (PRR), pulse width and burst length according to DeepRadar [38]. In Table 2, we give the typical configurations for five types of radar signals. As we present in Section 4.2.5, as long as one pulse in the burst is detected, we consider it as a radar detection event and count it as a true positive event; if no pulse in a burst is identified, we will count it as false positive events. Then we can calculate the TPR and FPR.

Table 2: Performance on radar detection

Radar type	Pulse width(us)	PRR length(ms)	Burst	TPR	FPR
1	2	1000	40	60%	0.5%
2	20	1000	20	98.6%	0.6%
3	4	1000	24	93.4%	0.8%
4	20	1000	8	85%	0.3%
5	75	1000	24	99%	0.8%

From the results, we can see that the pulse width and burst length are deterministic factors for signal detection. A shorter burst length indicates fewer radar pulses, which increases the probability of miss detection. This is evident by comparing the performance of Radar Type 2 and Radar Type 4. When the radar signal (Type 2) lasts for over 20ms, *WISE* can have enough time to detect at least one pulse, and the TPR can reach 98.6%. However, when the pulse width is shorter than 2μs (Type 1), even if the radar pulse occurs at the same time as the UWB preamble, we still have a high probability of miss detection. That is because DW1000 will accumulate the cross-correlation results of 64 symbols until saturation, the radar pulse whose duration is 2μs can be buried in those 64μs preamble symbols, resulting in a low SNR and thus miss detection. Another possible reason for miss detection is that the pulse may occur after the accumulation stops. The accumulator will stop accumulation either when the accumulator saturates or it grows quickly. The results in Table 2 show that *WISE* has good performance in detecting the majority of radar signals.

6.8 Transient Signal Detection

In addition to radar signals, there may be some fleeting/transient signals in the real world. It is necessary to evaluate the performance

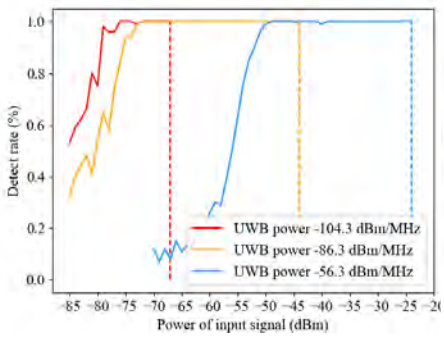

Figure 16: Sensitivity under different levels of UWB TX power

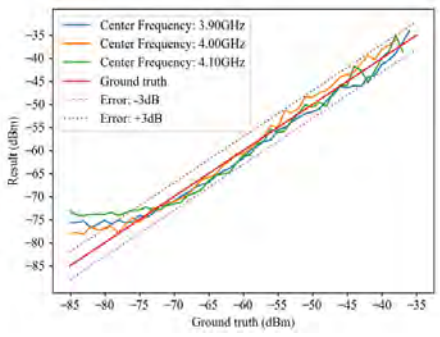

Figure 17: The performance of power estimation

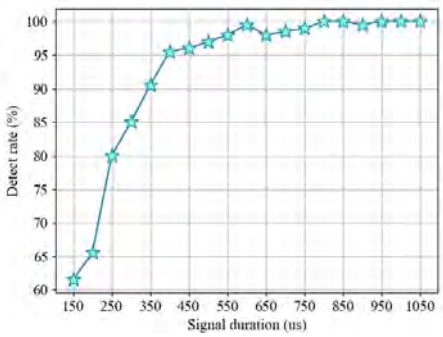

Figure 18: Transient signal detection

(a) Complex environment

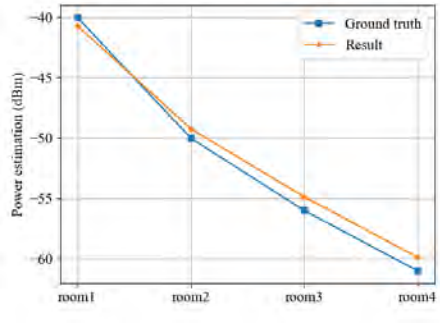

(b) The performance in complex environment

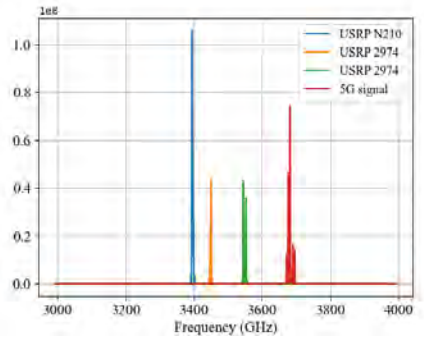

(c) The performance of detecting concurrent transmissions

Figure 19: Performance in complex environment

of *WISE* to detect those fleeting/transient signals. In this experiment, we generate test signals whose duration varies from 150µs to 1050µs, at 50µs granularity. We transmit the test signal every 50ms, and repeat it over 200 times. We record how many times *WISE* detects the signal. We define the detection rate of *WISE* as the ratio between the number of times that *WISE* successfully detects the signal and the actual number of signal occurrences. In this experiment, we configure *WISE* to work in radar mode.

Results are shown in Figure 18. As *WISE* has 500µs time interval between two detections, there is about 35% probability of missing the signal whose duration is shorter than 200µs. However, when the signal lasts longer than 400µs, there is 95% probability that the signal can be detected by *WISE*. *WISE* can detect the signal with nearly 100% probability when the signal duration is longer than 1ms. From the results, we can conclude that *WISE* can reliably detect signals which last longer than 400µs.

6.9 Complex environment

In order to test the performance in more challenging setups, we evaluate *WISE* in a through-the-wall scenario and with the presence of multiple active radios. For the through-the-wall experiment, the test environment is shown in Figure 19(a). In Room 1, we set a USRP N210 as the signal source which continuously transmits OFDM signal with 10 MHz bandwidth. Then we put *WISE* in different rooms to detect this signal and estimate its power. In order to obtain the ground truth, we use the RS FSH Handheld spectrum analyzer (9KHz-8GHz)[42] to estimate the signal power in the same place as *WISE* device. In each room, *WISE* conducts power measurement 400 times, and then we average the results of 400 measurements. Results are shown in Figure 19(b). Although the signal has penetrated through three walls from Room 1 to Room 4, *WISE* can still detect its presence and estimate its power with less than 1 dB error.

We also test the performance of *WISE* to detect concurrent transmissions of multiple radios. In this experiment, we use one USRP N210 and two TX channels of USRP 2974 to send OFDM signal with 10MHz bandwidth at center frequencies of 3.4 GHz (USRP N210), 3.45 GHz (channel 0 of USRP 2974), 3.55 GHz (channel 1 of USRP 2974), concurrently. At the same time, we use a 5G base station emulator (5GS-W500 from V3 technology) to transmit 5G signals at NR77/78 band (3.6 ~ 3.7 GHz). Then we use *WISE* to detect these four signals. The result is shown in Figure 19(c). We can see that *WISE* has successfully captured the signal at each corresponding frequency. Thus, *WISE* can work reliably when there are concurrent transmissions of multiple radios in the environment.

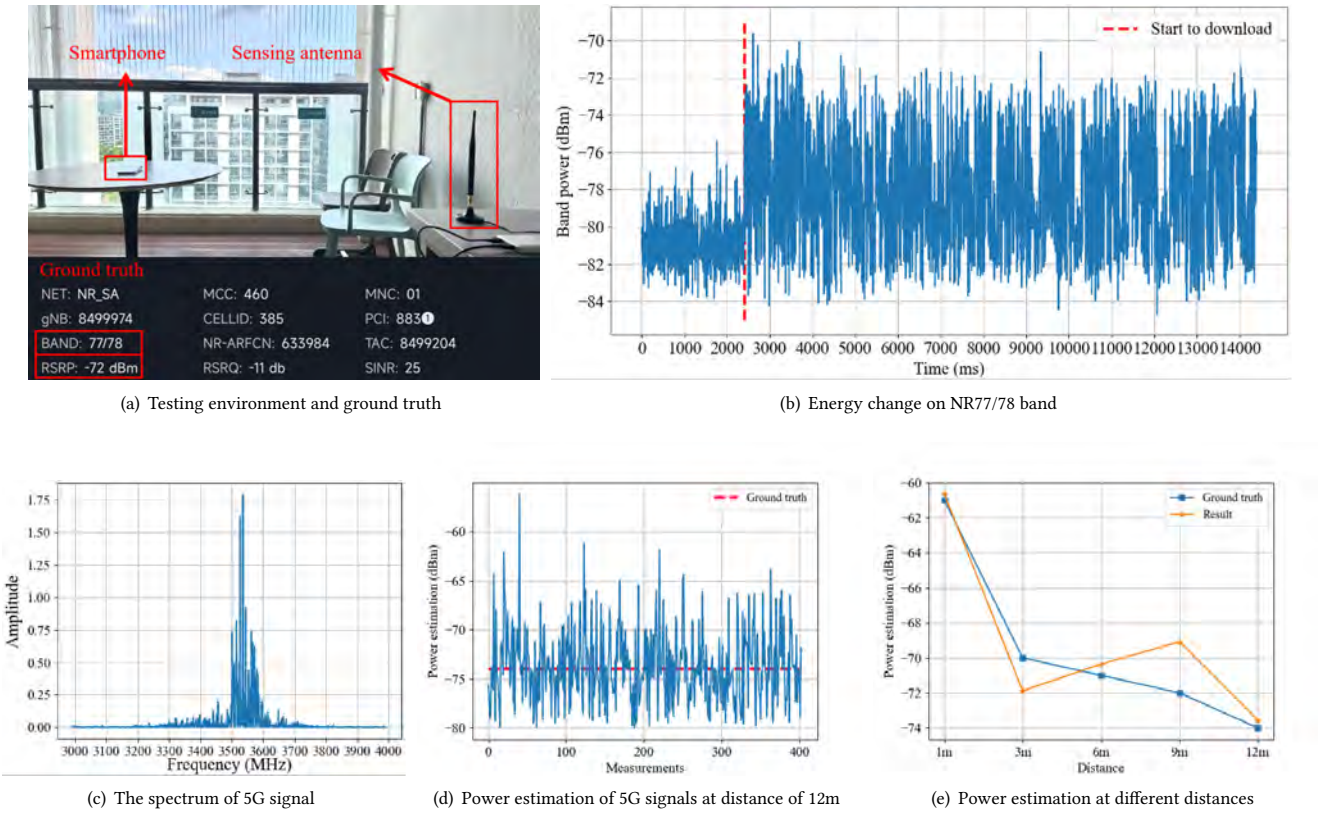

(a) Testing environment and ground truth

(b) Energy change on NR77/78 band

(c) The spectrum of 5G signal

(d) Power estimation of 5G signals at distance of 12m

(e) Power estimation at different distances

Figure 20: Performance of detecting 5G signals

6.10 5G Signal Detection

To evaluate the performance of *WISE* in the field, we attempt to detect in-air 5G signal with *WISE*. As shown in Figure 20(a), we put a Xiaomi 12 Pro 5G smartphone on a table which is about 2m from the *WISE* prototype. The smartphone is downloading a large file from the Internet. The connection information, i.e., the 5G band and signal power, is obtained from Speedtest. The details are also shown in Figure 20(b). We can see that the smartphone is working in NR77/78 band and the signal power is −72dBm.

The spectrum sensing result from *WISE* is shown in Figure 20(c). From the results, we can see that 3.5GHz ∼ 3.6GHz is occupied, which corresponds to the NR77/78 band. The power estimation result is shown in Figure 20(b). At about 2.2s, we start to download the file. *WISE* estimates the signal power to be around −73dBm, which is close to the information we obtain from Speedtest.

To more comprehensively demonstrate *WISE*'s ability to detect 5G signals, we use the 5G base station emulator, 5GS-W500 from V3 technology, to transmit 5G signals, and deploy *WISE* to detect 5G signals at different distances from the source. At each distance, *WISE* will estimate the signal power 400 times. In order to obtain the ground truth, we use the RS FSH Handheld spectrum analyzer (9KHz-8GHz) to estimate the signal power by taking the average value of multiple measurements at each distance. Then we average the results of 400 measurements from *WISE* and compare them with the ground truth. As the 5G signal is not a constant wave, where the active RUs keep changing, it results in the variation of the signal power, which is shown in Figure 20(d). Thus, it is hard to get accurate measurements of instantaneous 5G signal power. By averaging over a time period, the power estimation from *WISE* deviates less than 3dB from the spectrum analyzer, which is shown in Figure 20(e).

From these results, we can conclude that *WISE* can reliably detect 5G signal and accurately estimate its power, which implies that *WISE* can help with strategic spectrum planning and allocations. Thanks to its low cost and wideband nature, it is feasible to deploy *WISE* at a city scale for fine-grained spectrum measurement.

7 RELATED WORKS

7.1 UWB Sensing

In recent years, UWB technology has become popular in both academics and industry. Thanks to its low cost and wideband nature, UWB has good performance in localization and sensing. On one hand, UWB technology has been used in indoor positioning [2, 6, 11, 16, 21, 22]. As the positioning accuracy of UWB can be of centimeter level, it can be used to track a writing trajectory of a pen [6], track the firefighters in buildings from outside [16], and track a ball's 3D trajectory for sports analytics [21]. On the other hand, UWB has also been used for pervasive RF sensing

[9, 10, 17, 31, 40, 44, 48, 49]. Octopus [10], a UWB MIMO sensing platform, has superior performance in passive localization, vibration sensing, and human/object imaging. Similarly, MoRe-Fi [9, 49], another UWB radar, employs deep contrastive learning to detect vital signs (particularly heartbeat and breath) despite the interference caused by body movements. SiWa [48] uses the UWB signal to identify the internal structure of the wall without breaking it; LiquID [17] can distinguish different types of liquids using the time-of-flight of signals to calculate the dielectric constant of liquids. In short, UWB has great potential in RF sensing.

UWB technology has also been integrated into many commercial products, such as smartphones (e.g., iPhone 11/12 Pro, Galaxy Note 20 Ultra) and IoT devices (e.g., Air tag). We expect that UWB devices will be pervasive in daily life. We envision that one day, these UWB devices are not only used for positioning or sensing, but also integrated with *WISE* for spectrum sensing. Thus, these smartphone and IoT devices may become spectrum sensors for city-level spectrum sensing.

7.2 Wideband Spectrum Sensing

Spectrum sensing is important for dynamic spectrum allocation. The authors in [33, 35, 36, 47] have built a sensor for large-scale spectrum monitoring. The spectrum sensor is built upon the low-cost commercial off-the-shelf (COTS) platform (i.e., RTL-SDR USB Dongle[35]). The total cost per sensor device is below $100. Similarly, Snoopy [47] uses commercial WiFi chipsets and RF frequency translators to build a low-cost spectrum sensor. However, those low-cost spectrum sensors have narrow bandwidth (e.g., 2MHz for RTL-SDR USB Dongle, 20MHz for WiFi). In order to cover a wide spectrum, they need to hop over different bands, which leads to poor time resolution. According to the Nyquist sampling theory, wideband spectrum sensing requires high-speed ADCs, which are too expensive to be widely affordable. To monitor a 500MHz band, a 1GHz ADC is required, which costs hundreds of dollars. Recent research focuses on wideband spectrum sensing using narrowband devices with signal processing techniques (e.g., sparse Fourier transform) [20, 25, 26] or some intelligent scanning algorithms [8, 24, 39, 46]. BigBand [26] uses the sparse Fourier transform to sense a wide bandwidth (e.g., 900MHz), when the spectrum is sparse or the changes of the spectrum are sparse. Due to the unprecedented number of wireless devices, the assumption that the spectrum is sparsely occupied may no longer hold. SpecInsight [39] can sense multi-GHz bands with 40MHz USRPs. Instead of sequentially scanning the whole band, SpecInsight will sense the channels that are likely to be active with high priority. Based on signal usage patterns, the authors use machine learning to predict spectrum occupancy. It works for known signal patterns, but for unpredictable signals, the performance of SpecInsight will degrade. SweepSense [24] can sweep the multi-GHz bands within several milliseconds by tuning the center frequency of USRP quickly. However, SweepSense also has poor performance when the spectrum is not sparse [23]. S^3 designs spike-train like filters based on MEMS acoustic resonators, which can sparsity the spectrum and enable sub-Nyquist rate sampling [23]. S^3 can sense over 500MHz bandwidth at once with two low-speed ADCs. However, the spike-train filters are customized, which are not ready for mass production.

In Table 3, we compare *WISE* with other spectrum sensing methods in terms of time resolution, sensitivity, and cost. From Table 3 we can see that, *WISE* is not as sensitive as the other spectrum sensing methods, however the high time resolution and low cost make *WISE* outstanding among all the sensing methods.

In summary, the current wideband spectrum monitoring techniques have clear limitations. In our work, we enable wideband spectrum monitoring with low-cost, commercial off-the-shelf UWB chips. Different from existing low-cost spectrum sensors, *WISE* not only can sense a wide spectrum, but also has high accuracy, good time resolution, and wide dynamic range. It can also detect fleeting signals like radar.

8 DISCUSSION

Here, we discuss the remaining issues in *WISE* and present possible countermeasures. First, in the current *WISE* design, there is 500µs between two detections. As we show in Section 6.8, *WISE* may miss fleeting signals that are shorter than 400µs. To address this problem, instead of setting a fixed inter-packet interval, we can improve *WISE* by configuring the inter-packet interval according to the Poisson distribution. The PASTA (Poisson Arrivals See Time Averages) property states that observations made of a system at time instants obeying a Poisson process, when averaged, converge to give the true value [5]. It will be our future work to validate Poisson sampling in *WISE*.

Second, the signal power that *WISE* can detect depends on the TX power of the excitation block. If the TX power is low, the high-power external signal may lead to failure in UWB packet detection and thus no valid CIR; if the TX power is high, the external signal will be buried in the UWB signals and leads to poor signal quality. From Section 6.5, *WISE* can sense signals ranging from −85dBm/MHz to −34dBm/MHz, which is limited by the 30dB range of DW1000 transmission gain. In order to further extend this range, we can replace the current 15dB attenuator with a digital variable attenuator. *WISE* can dynamically adjust the attenuator so that we can extract the in-air signals with good quality. Furthermore, we can add a power amplifier between the receiving antenna and the combiner to amplify external signals, so as to improve the sensitivity of *WISE* and enable it to sense weak signals.

Third, the frequency range of *WISE* is limited by the UWB chip. In this paper, we built *WISE* with DW1000, which supports six bands from 3.1GHz to 7GHz. It covers the 3.5GHz CBRS band (coexistence of LTE and military radar) and the unlicensed 6GHz band (coexistence of Wi-Fi 6E and 5G). FCC authorized the unlicensed use of UWB in the frequency range from 3.1GHz to 10.6GHz. CEVA [7] from RivieraWaves UWB supports a wider frequency range than DW1000, from 3.1GHz to 10.6GHz. We can extend the frequency range of *WISE* by replacing DW1000 with CEVA. To further extend the frequency range, we can add a frequency translator to up-convert/down-convert the signals into the frequency range of the UWB chip. In this way, we can enable *WISE* to support a larger frequency range.

Finally, as most commercial products such as smartphones (e.g., iPhone 11/12 Pro [3, 43]) and IoT devices (e.g., Air tag [1]) do not provide APIs for their UWB chips, it would be our future work to try to use these commercial products for spectrum sensing. For

Table 3: Comparison between *WISE* and other state-of-the-art spectrum sensing methods

	Time resolution	Sensitivity	Cost
Bigband	900 MHz / (100 us ~ 10 ms)	-100 dBm	~ $3000 (USRP-N210)
SweepSense	153 MHz / 1 ms	-60 dBm	~ $3000 (USRP-N210)
BeyondSensing [39]	50 MHz / 50 ms	-100 dBm	~ $3000 (USRP-N210)
S^3	418 MHz / (40 ~ 100 us)	SNR>3dB	N/A
RTL-Dongle [35]	2 MHz / 66 ms	-90 dBm	< $100
WI-SPY [32]	100 MHz / 250 ms	-95 dBm	~ $100
WISE	900 MHz / (500 us ~ 2 ms)	-75 dBm	~ $100

example, we can use a smartphone/IoT device as the transmitter, and another two smartphones/IoT devices as the receivers, so they work collaboratively as a spectrum sensor. It may encourage mobile users to participate in spectrum sensing in a crowd-sourcing manner.

9 CONCLUSION

In this paper, we present how we transform UWB chipsets into a spectrum sensor. We introduce the design of *WISE*, a lost-cost wideband spectrum sensing unit, which is built with the commercial off-the-shelf UWB chip, DW1000. *WISE* can sense up to 900MHz bandwidth without using expensive high-speed ADCs. *WISE* exploits the channel impulse response to obtain the spectrum occupancy information. We implement *WISE* and extensively evaluate its performance. Results show that *WISE* can accurately detect spectrum occupancy and estimate the signal power/bandwidth with high precision. *WISE* can also detect fleeting radar signals. We also demonstrate *WISE* with a field test, where *WISE* can accurately detect 5G signals and estimate 5G signal power. We believe that *WISE* brings a new paradigm for spectrum sensing. As UWB chipsets are becoming popular on smartphones and IoT devices, we expect that in the future, these commodity devices may participate in city-level spectrum sensing.

ACKNOWLEDGEMENTS

We are truly grateful to all the anonymous reviewers for their insightful comments. This research is supported in part by the Key-Area Research and Development Program of Guangdong Province (No. 2020B0101390001), in part by the National Natural Science Foundation of China (No. 62002150), in part by RGC under Contract CERG 16203719, Contract 16204820, and Contract R8015, and in part by The Major Key Project of PCL(PCL2021A15). Q. Huang is the corresponding author.

REFERENCES

[1] AirTag 2021. Apple AirTag arrives for $29, uses Ultra Wideband and does Emoji. https://www.gsmarena.com/apple_airtag_finally_arrives_for_29_uses_ultrawideband_and_does_emoji-news-48753.php

[2] Boyd Anderson, Mingqian Shi, Vincent YF Tan, and Ye Wang. 2019. Mobile gait analysis using foot-mounted UWB sensors. *Proceedings of the ACM on Interactive, Mobile, Wearable and Ubiquitous Technologies* 3, 3 (2019), 1–22.

[3] Apple U1 chip 2020. Apple U1 chip explained: What is it and what can it do? https://www.pocket-lint.com/phones/news/apple/149336-how-apple-s-u1-chip-adds-amazing-new-capabilities-to-the-iphone

[4] Apple watch 2020. Apple Watch Series 6 Features U1 Chip for Ultra Wideband. https://www.macrumors.com/2020/09/15/apple-watch-series-6-u1-chip-ultra-wideband/

[5] Francçois Baccelli, Sridhar Machiraju, Darryl Veitch, and Jean C Bolot. 2006. The role of PASTA in network measurement. *ACM SIGCOMM Computer Communication Review* 36, 4 (2006), 231–242.

[6] Yifeng Cao, Ashutosh Dhekne, and Mostafa Ammar. 2021. ITrackU: tracking a pen-like instrument via UWB-IMU fusion. In *Proceedings of the 19th Annual International Conference on Mobile Systems, Applications, and Services*. 453–466.

[7] CEVA-RivieraWaves UWB 2011. Low power ultra-wideband IP for Mobile, Automotive, Consumer and IoT applications. https://www.ceva-dsp.com/product/rivierawaves-uwb-platform/

[8] Ayon Chakraborty, Md Shaifur Rahman, Himanshu Gupta, and Samir R Das. 2017. Specsense: Crowdsensing for efficient querying of spectrum occupancy. In *IEEE INFOCOM 2017-IEEE Conference on Computer Communications*. IEEE, 1–9.

[9] Zhe Chen, Tianyue Zheng, Chao Cai, and Jun Luo. 2021. MoVi-Fi: Motion-robust vital signs waveform recovery via deep interpreted RF sensing. In *Proceedings of the 27th Annual International Conference on Mobile Computing and Networking*. 392–405.

[10] Zhe Chen, Tianyue Zheng, and Jun Luo. 2021. Octopus: a practical and versatile wideband MIMO sensing platform. In *Proceedings of the 27th Annual International Conference on Mobile Computing and Networking*. 601–614.

[11] Pablo Corbalán, Gian Pietro Picco, and Sameera Palipana. 2019. Chorus: UWB concurrent transmissions for GPS-like passive localization of countless targets. In *2019 18th ACM/IEEE International Conference on Information Processing in Sensor Networks (IPSN)*. IEEE, 133–144.

[12] Decawave 2014. *Wireless Sensor Networks And The DW1000.* Decawave. https://www.decawave.com/wp-content/uploads/2018/10/APS010_DW1000-and-Wireless-Sensor-Networks_v1.1.pdf.

[13] Decawave 2015. *DW1000 Data Sheet.* Decawave. https://www.decawave.com/sites/default/files/resources/dw1000-datasheet-v2.09.pdf.

[14] Decawave 2017. *DW1000 User manual.* Decawave. https://www.decawave.com/sites/default/files/resources/dw1000_user_manual_2.11.pdf.

[15] Decawave 2018. *EVK1000 User manual.* Decawave. https://www.decawave.com/wp-content/uploads/2018/09/evk1000_user_manual.pdf.

[16] Ashutosh Dhekne, Ayon Chakraborty, Karthikeyan Sundaresan, and Sampath Rangarajan. 2019. TrackIO: Tracking First Responders Inside-Out. In *16th USENIX Symposium on Networked Systems Design and Implementation (NSDI 19)*. 751–764.

[17] Ashutosh Dhekne, Mahanth Gowda, Yixuan Zhao, Haitham Hassanieh, and Romit Roy Choudhury. 2018. Liquid: A wireless liquid identifier. In *Proceedings of the 16th Annual International Conference on Mobile Systems, Applications, and Services*. 442–454.

[18] Federal Communications Commission 2020. 3.5 GHz Band Overview. https://www.fcc.gov/35-ghz-band-overview

[19] Federal Communications Commission 2020. FCC Opens 6 GHz Band to Wi-Fi and Other Unlicensed Uses. https://www.fcc.gov/document/fcc-opens-6-ghz-band-wi-fi-and-other-unlicensed-uses-0

[20] Badih Ghazi, Haitham Hassanieh, Piotr Indyk, Dina Katabi, Eric Price, and Lixin Shi. 2013. Sample-optimal average-case sparse fourier transform in two dimensions. In *2013 51st Annual Allerton Conference on Communication, Control, and Computing (Allerton)*. IEEE, 1258–1265.

[21] Mahanth Gowda, Ashutosh Dhekne, Sheng Shen, Romit Roy Choudhury, Lei Yang, Suresh Golwalkar, and Alexander Essanian. 2017. Bringing IoT to Sports Analytics. In *14th USENIX Symposium on Networked Systems Design and Implementation (NSDI 17)*. 499–513.

[22] Bernhard Großwindhager, Michael Rath, Josef Kulmer, Mustafa S Bakr, Carlo Alberto Boano, Klaus Witrisal, and Kay Römer. 2018. SALMA: UWB-based single-anchor localization system using multipath assistance. In *Proceedings of the 16th ACM Conference on Embedded Networked Sensor Systems*. 132–144.

[23] Junfeng Guan, Jitian Zhang, Ruochen Lu, Hyungjoo Seo, Jin Zhou, Songbin Gong, and Haitham Hassanieh. 2021. Efficient Wideband Spectrum Sensing Using MEMS Acoustic Resonators. In *18th USENIX Symposium on Networked Systems Design and Implementation (NSDI 21)*. 809–825.

[24] Yeswanth Guddeti, Raghav Subbaraman, Moein Khazraee, Aaron Schulman, and Dinesh Bharadia. 2019. SweepSense: Sensing 5 GHz in 5 Milliseconds with Low-cost Radios. In *16th USENIX Symposium on Networked Systems Design and Implementation (NSDI 19)*. 317–330.

[25] Haitham Hassanieh, Piotr Indyk, Dina Katabi, and Eric Price. 2012. Nearly optimal sparse Fourier transform. In *Proceedings of the forty-fourth annual ACM symposium on Theory of computing*. 563–578.

[26] Haitham Hassanieh, Lixin Shi, Omid Abari, Ezzeldin Hamed, and Dina Katabi. 2014. GHz-wide sensing and decoding using the sparse Fourier transform. In *IEEE INFOCOM 2014-IEEE Conference on Computer Communications*. IEEE, 2256–2264.

[27] IEEE Standard 802.15.4-2011 2011. IEEE Standard for Local and metropolitan area networks–Part 15.4: Low-Rate Wireless Personal Area Networks (LR-WPANs). https://standards.ieee.org/ieee/802.15.4/5050/

[28] Keysight 2021. *Keysight M8190A arbitrary waveform generator*. Keysight. https://www.keysight.com/hk/en/assets/7018-02903/data-sheets/5990-7516.pdf.

[29] Keysight 2022. *E8267D PSG Vector Signal Generator*. Keysight. https://www.keysight.com/hk/en/assets/7018-01210/data-sheets/5989-0697.pdf.

[30] Keysight 2022. *PathWave System Design (SystemVue)*. Keysight. https://www.keysight.com/hk/en/products/software/pathwave-design-software/pathwave-system-design-software.html.

[31] Yongsen Ma, Yunze Zeng, and Vivek Jain. 2020. CarOSense: Car occupancy sensing with the ultra-wideband keyless infrastructure. *Proceedings of the ACM on Interactive, Mobile, Wearable and Ubiquitous Technologies* 4, 3 (2020), 1–28.

[32] Metageek 2022. *WI-SPY datasheet*. Metageek. https://support.metageek.com/hc/en-us/articles/360016560613-Wi-Spy-Air-Hardware-Data-Sheet.

[33] Ana Nika, Zhijing Li, Yanzi Zhu, Yibo Zhu, Ben Y Zhao, Xia Zhou, and Haitao Zheng. 2016. Empirical validation of commodity spectrum monitoring. In *Proceedings of the 14th ACM Conference on Embedded Network Sensor Systems*. 96–108.

[34] Ana Nika, Zengbin Zhang, Xia Zhou, Ben Y Zhao, and Haitao Zheng. 2014. Towards commoditized real-time spectrum monitoring. In *Proceedings of the 1st ACM Workshop on Hot Topics in Wireless*. 25–30.

[35] Damian Pfammatter, Domenico Giustiniano, and Vincent Lenders. 2015. A software-defined sensor architecture for large-scale wideband spectrum monitoring. In *Proceedings of the 14th International Conference on Information Processing in Sensor Networks*. 71–82.

[36] Sreeraj Rajendran, Roberto Calvo-Palomino, Markus Fuchs, Bertold Van den Bergh, Héctor Cordobés, Domenico Giustiniano, Sofie Pollin, and Vincent Lenders. 2017. Electrosense: Open and big spectrum data. *IEEE Communications Magazine* 56, 1 (2017), 210–217.

[37] Samsung Galaxy Note20 2020. NXP Secure UWB deployed in Samsung Galaxy Note20 Ultra Bringing the First UWB-Enabled Android Device to Market | NXP Semiconductors - Newsroom. https://media.nxp.com/news-releases/news-release-details/nxp-secure-uwb-deployed-samsung-galaxy-note20-ultra-bringing/

[38] Shamik Sarkar, Milind Buddhikot, Aniqua Baset, and Sneha Kumar Kasera. 2021. DeepRadar: A deep-learning-based environmental sensing capability sensor design for CBRS. In *Proceedings of the 27th Annual International Conference on Mobile Computing and Networking*. 56–68.

[39] Lixin Shi, Paramvir Bahl, and Dina Katabi. 2015. Beyond Sensing:Multi-GHz Realtime Spectrum Analytics. In *12th USENIX Symposium on Networked Systems Design and Implementation (NSDI 15)*. 159–172.

[40] Mridula Singh, Patrick Leu, AbdelRahman Abdou, and Srdjan Capkun. 2019. UWB-ED: Distance Enlargement Attack Detection in Ultra-Wideband. In *28th USENIX Security Symposium (USENIX Security 19)*. 73–88.

[41] SmartTag 2021. Samsung's Galaxy SmartTag is a $29.99 Tile competitor. https://www.theverge.com/2021/1/14/22227621/samsung-galaxy-smarttag-price-release-date-tile-locator

[42] Spectrum Analyzers 2022. RS FSH Handheld spectrum analyzer. https://www.rohde-schwarz.com/us/products/test-and-measurement/handheld/rs-fsh-handheld-spectrum-analyzer_63493-8180.html

[43] U1 chip in iphone11 2019. The U1 chip in the iPhone 11 is the beginning of an Ultra Wideband revolution. https://sixcolors.com/post/2019/09/the-u1-chip-in-the-iphone-11-is-the-beginning-of-an-ultra-wideband-revolution/

[44] Ziqi Wang, Zhe Chen, Akash Deep Singh, Luis Garcia, Jun Luo, and Mani B Srivastava. 2020. UWHear: through-wall extraction and separation of audio vibrations using wireless signals. In *Proceedings of the 18th Conference on Embedded Networked Sensor Systems*. 1–14.

[45] Xiaomi Mix4 2021. NXP Trimension™ Ultra-Wideband Technology Powers Xiaomi MIX4 Smartphone to Deliver New "Point to Connect" Smart Home Solution. https://www.globenewswire.com/news-release/2021/09/27/2303266/0/en/NXP-Trimension-Ultra-Wideband-Technology-Powers-Xiaomi-MIX4-Smartphone-to-Deliver-New-Point-to-Connect-Smart-Home-Solution.html

[46] Sungro Yoon, Li Erran Li, Soung Chang Liew, Romit Roy Choudhury, Injong Rhee, and Kun Tan. 2013. QuickSense: Fast and energy-efficient channel sensing for dynamic spectrum access networks. In *2013 Proceedings IEEE INFOCOM*. IEEE, 2247–2255.

[47] Tan Zhang, Ashish Patro, Ning Leng, and Suman Banerjee. 2015. A wireless spectrum analyzer in your pocket. In *Proceedings of the 16th International Workshop on Mobile Computing Systems and Applications*. 69–74.

[48] Tianyue Zheng, Zhe Chen, Jun Luo, Lin Ke, Chaoyang Zhao, and Yaowen Yang. 2021. SiWa: see into walls via deep UWB radar. In *Proceedings of the 27th Annual International Conference on Mobile Computing and Networking*. 323–336.

[49] Tianyue Zheng, Zhe Chen, Shujie Zhang, Chao Cai, and Jun Luo. 2021. MoRe-Fi: Motion-robust and Fine-grained Respiration Monitoring via Deep-Learning UWB Radar. In *Proceedings of the 19th ACM Conference on Embedded Networked Sensor Systems*. 111–124.